Available online at www.sciencedirect.com
ScienceDirect
Journal of Sound and Vibration 309 (2008) 600–612
JOURNAL OF SOUND AND VIBRATION
www.elsevier.com/locate/jsvi

Vibrations of narrow microbeams predeformed by an electric field

R.C. Batra[a,*], M. Porfiri[b], D. Spinello[a]

[a]Department of Engineering Science and Mechanics, MC 0219, Virginia Polytechnic Institute and State University, Blacksburg, VA 24061, USA
[b]Department of Mechanical, Aerospace and Manufacturing Engineering, Polytechnic University, Brooklyn, NY 11201, USA

Received 11 July 2006; received in revised form 2 February 2007; accepted 24 July 2007
Available online 12 September 2007

Abstract

Vibrations of a fixed–fixed narrow microbeam electrostatically actuated by applying a voltage difference to it and a parallel rigid conductor are analyzed. For gaps between the two conductors that are comparable to the beam's thickness, the fundamental frequency of the beam may first increase with increasing applied voltage, before suddenly dropping at the pull-in voltage. Available models fail to accurately describe this behavior of the frequency versus voltage diagram for narrow microbeams, that results from a combination of strain-hardening and electrostatic softening effects. A distributed electromechanical model, that accounts for electrostatic fringing fields, finite deflections and residual stresses, is proposed. A recent estimate of the electrostatic force incorporating fringing fields due to both finite width and finite thickness of the microbeam is employed. The lowest frequency is extracted with a simple and computationally efficient one degree-of-freedom model obtained by approximating the deflection field with the static deflection of a fixed–fixed microbeam loaded by a uniformly distributed force. The model's predictions are in good agreement with those from three-dimensional finite-element simulations.

1. Introduction

Electrostatically actuated microbeams are extensively used as microelectromechanical systems (MEMS) and resonant sensors in different applications such as signal filtering, and chemical and mass sensing; see Refs. [1–9]. An electrostatically actuated microbeam is an elastic beam suspended above a stationary rigid plate. Both bodies are made of electrically conductive materials, and a dielectric medium fills the gap between them. For a resonant sensor, a direct current (D.C.) voltage applied across the microbeam and the rigid plate deflects the microbeam and an alternating current (A.C.) harmonic voltage applied across the two conductors forces the microbeam to vibrate. For A.C. voltage amplitudes much smaller than the D.C. voltage the microbeam resonance frequencies are controlled by the D.C. voltage. Zook et al. [10] observed experimentally that increasing the driving A.C. voltage enhances the resonance frequency (hardening effect). In Refs. [2,5,8]

*Corresponding author.
E-mail addresses: rbatra@vt.edu (R.C. Batra), mporfiri@poly.edu (M. Porfiri), dspinell@vt.edu (D. Spinello).

0022-460X/$ - see front matter © 2007 Elsevier Ltd. All rights reserved.
doi:10.1016/j.jsv.2007.07.030

the model developed in Ref. [1] is used for analyzing nonlinear oscillations due to moderately large applied A.C. voltages.

The applied D.C. voltage has an upper limit beyond which the electrostatic force is not balanced by the elastic restoring force in the deformable beam, the beam spontaneously deflects towards the stationary rigid plate, and the device collapses. This instability, known as the pull-in instability, was simultaneously observed experimentally by Taylor [11] and Nathanson et al. [12]. The accurate characterization of the pull-in instability represents a focal point of research in the MEMS community, see Ref. [13].

A comprehensive review of different models of electrostatically actuated microbeams and their predictions is given in Refs. [14,27]. In Ref. [4], vibrations of a wide clamped–clamped microbeam are studied using the classical linear beam theory and discarding all fringing field effects. Experimental results are in good agreement with theoretical findings for moderately small deflections. In Ref. [1], the microbeam model is improved by considering mid-plane stretching; this gives good values of the fundamental frequency for applied voltages close to that for the pull-in instability. The effect of increasing the gap between the microbeam and the parallel rigid plate is considered, and it is shown that for considerably large gaps the fundamental frequency may increase with increasing voltages before reaching the pull-in instability. In Ref. [7], the nonlinear mechanical model of Ref. [1] is further improved by considering effects of fringing fields due to beam's finite width according to Palmer's formula [15]. The fringing field correction seems to be first considered in the MEMS literature in Ref. [16], where the model of Ref. [4] was supplemented with Palmer's formula for extracting the pull-in parameters. However, as noticed in Ref. [17], and also observed in Ref. [18], none of these works is applicable to narrow microbeams where fringing field effects due to the finite thickness are not negligible.

Numerical extraction of pull-in parameters and frequencies of vibration require the solution of stiff nonlinear ordinary differential equations. Several techniques have been proposed in the literature for finding accurate numerical solutions, for example the shooting method [1], the differential quadrature method [7], the finite element method [18], the meshless local Petrov–Galerkin method [18], the Rayleigh–Ritz method [4], the Galerkin method using microbeam's mode shapes and perturbation techniques [19] or the static microbeam's deflections under appropriate loads [18].

Here, we study vibrations of narrow microbeams predeformed by an electric field with the electromechanical model of Ref. [18] that estimates the electrostatic fringing field due to both the finite width and the finite thickness of the microbeam. In Ref. [18], it is shown that for relatively narrow microbeams, the work presented in Ref. [1] considerably overestimates the pull-in voltage and underestimates the pull-in maximum displacement, while the version proposed in Ref. [7] overestimates both the pull-in voltage and the pull-in maximum deflection. We show here similar differences in microbeam's fundamental frequency. In particular, we show that the model of Ref. [1], by underestimating microbeam's displacements, underestimates the mechanical nonlinear hardening and consequently underestimates microbeam's fundamental frequency. In addition, we show that its modified version [7], by overestimating microbeam's displacements, overestimates the nonlinear mechanical hardening and therefore microbeam's fundamental frequency. We show that the model proposed in Ref. [18] overcomes these shortcomings and is suitable for accurately predicting the vibrational response of the microbeam. We perform a three-dimensional (3-D) finite element simulation for verifying our results and show quantitative discrepancies among predictions from models of Refs. [1,7,16] with the finite element findings, and the relevant qualitative differences may appear in the frequency versus voltage diagram. Numerical results are obtained by using the one degree-of-freedom model proposed in Ref. [18], and based on approximating microbeam's deflection with the static deflection under a uniformly distributed load. The present reduced order one degree-of-freedom model differs from the classical mass-spring system of Ref. [12], since we account for the axial stress, nonlinear stiffening, charge redistribution, and fringing fields. It also differs from that of Ref. [19] since we retain the complete nonlinear behavior of the electrostatic force and consider fringing fields, and it differs from that of Ref. [17] since we simultaneously treat the pull-in voltage and the pull-in deflection as unknowns, i.e., the pull-in deflection is not empirically chosen as was done in Ref. [17]. The one degree-of-freedom model is validated by showing that its predictions are in good agreement with those from the multimode analysis [1,9], with pull-in parameters extracted by combining the Galerkin method with the displacement pull-in extraction (DIPIE) [20] algorithm.

The rest of the paper is organized as follows. In Sections 2 and 3 we describe, respectively, the electromechanical model and the one degree-of-freedom models. In Section 4 we provide details of the 3-D finite element simulations performed with the commercial code ANSYS. In Section 5 we compare our results with those from other models in the literature and also with results of the 3-D finite element simulations. We further validate the one degree-of-freedom model by comparing its predictions with those of a multimode analysis. Conclusions are summarized in Section 6.

2. Governing equations

We consider a clamped–clamped narrow microbeam of length ℓ, width b, and thickness h, as depicted in Fig. 1. The microbeam is suspended above an infinite ground plane with an initial gap g_0. Both bodies are perfect conductors and are separated by a dielectric medium of permittivity $\varepsilon_0\varepsilon_r$, where ε_0 is the vacuum permittivity, and ε_r is the relative permittivity. A positive potential difference V between the two conductors causes the microbeam to deflect.

2.1. Nonlinear equation for beam's large deflections

We incorporate the von Kármán nonlinearity in the expression for the axial strain to account for large deflections, large rotations and small strains of the narrow beam; see Ref. [21]. The deflection w (see Fig. 1) in the z-direction is governed by

$$\varrho bh\ddot{w} + EIw^{IV} - N(w)w'' = F_e(w), \tag{1}$$

where ϱ is the mass density, E the Young's modulus, I the moment of inertia of the cross-section about the y-axis, N the axial force for a given deflection $w(x,t)$ of the beam, F_e the deflection-dependent electrostatic force per unit length, x the axial coordinate, and t the time. A superimposed dot means time derivative, while a prime signifies spatial derivative with respect to the axial coordinate x. Effects of transverse shear stresses are neglected since for a typical microbeam $\ell/h > 20$. A beam is considered narrow, when its width b is less than five times its thickness h, see Ref. [16]. For a wide beam, the mechanical stiffness EI should be modified as given in Ref. [16], where an effective Young's modulus is considered. The axial force is given by

$$N(w) = \frac{Ebh}{2\ell}\int_0^\ell (w')^2\,\mathrm{d}x + N_0, \tag{2}$$

where N_0 is the initial axial load. For a narrow beam, $N_0 = \tilde{\sigma}A$, where $\tilde{\sigma} = \sigma_0(1-\nu)$, σ_0 is the initial uniform biaxial stress in the material, and ν is the Poisson's ratio; see Ref. [16].

The beam deflection is subjected to the following four kinematic boundary conditions:

$$w(0,t) = 0, \quad w'(0,t) = 0, \quad w(\ell,t) = 0, \quad w'(\ell,t) = 0. \tag{3}$$

No initial conditions are needed for studying the free-vibration problem. Here we focus on analyzing deformations of the beam in the xz plane.

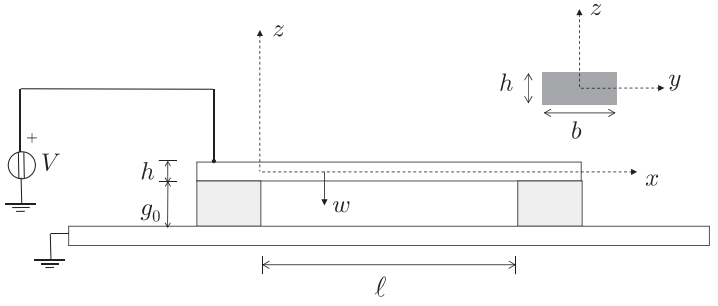

Fig. 1. Sketch of the electrostatically actuated device.

2.2. Electrostatic load

The distributed force, $F_e(w)$, on the deformable microbeam due to the electric field depends on the potential difference between the two conductors, the gap between them and on their geometries. Since only small strains in the beam are considered, it is reasonable to assume that at every point x of the beam the electrostatic force per unit length, F_e, depends only on the local deflection $w(x,t)$ and equals the force per unit length acting on an infinitely long straight beam separated by a distance $g(x,t) = g_0 - w(x,t)$ from a ground plane as shown in Fig. 1. The force F_e is computed by differentiating with respect to the gap g the energy per unit length stored in the capacitor, that is

$$F_e = -\frac{1}{2} V^2 \frac{\partial C_g}{\partial g}. \tag{4}$$

Here C_g is the capacitance per unit length of the 2-D conductors' system, and V is the voltage difference between the two bodies. The capacitance C_g is comprised of the parallel-plate capacitance, and the fringing field capacitance due to the finite width and the finite thickness of the beam.

It is shown in Ref. [18] that for narrow microbeams with $0.2 \leqslant h/b \leqslant 2$ and $0.4 \leqslant h/g \leqslant 5$ the capacitance C_g is estimated within 2% error, with respect to a fully converged numerical solution, by

$$\frac{C_g}{\varepsilon_0 \varepsilon_r} = \frac{b}{g} - 0.36 + 0.85\left(\frac{b}{g}\right)^{0.24} + 2.5\left(\frac{h}{g}\right)^{0.24}. \tag{5}$$

Substituting for C_g from Eq. (5) into Eq. (4) we obtain

$$F_e = \frac{\varepsilon_0 \varepsilon_r}{2} \frac{b V^2}{(g_0 - w)^2} \mathscr{F}, \tag{6}$$

where the nondimensional fringing field correction factor $\mathscr{F}$ is given by

$$\mathscr{F} = 1 + 0.204\left(\frac{g_0 - w}{b}\right)^{0.76} + 0.6\frac{h}{b}\left(\frac{g_0 - w}{h}\right)^{0.76}. \tag{7}$$

The parallel-plate approximation of the electrostatic force is characterized by $\mathscr{F} = 1$. The second term on the right-hand side of Eq. (7) accounts for the finite width of the beam, and the third term for the finite thickness of the beam. An improved estimate of the capacitance is given in Ref. [28].

3. One degree-of-freedom model

A closed-form solution of the vibration problem defined by Eqs. (1), (2), (6) and boundary conditions in Eq. (3) cannot be found. Here we give an approximate solution based on a one degree-of-freedom model of the MEMS. The approximate solution is constructed by expressing the deflection field $w(x,t)$ as the product of an unknown nondimensional time-dependent deflection parameter $\zeta(t)$, and a trial function $\bar{w}(x)$ satisfying the kinematic boundary conditions in Eq. (3):

$$w(x,t) = \zeta(t)\bar{w}(x). \tag{8}$$

The governing equation for $\zeta(t)$ is derived by multiplying both sides of Eq. (1) with $\bar{w}$, integrating the resulting equation over the beam span, and substituting into it the approximate solution given by Eq. (8):

$$\begin{aligned} &\int_0^\ell \varrho bh\ddot{\zeta}\bar{w}^2 \,\mathrm{d}x + \int_0^\ell EI\zeta\bar{w}^{IV}\bar{w}\,\mathrm{d}x \\ &\quad - \left(\frac{Ebh}{2\ell}\int_0^\ell (\zeta\bar{w}')^2\,\mathrm{d}x + N_0\right)\int_0^\ell \zeta\bar{w}''\bar{w}\,\mathrm{d}x \\ &\quad = \int_0^\ell F_e(\zeta\bar{w})\bar{w}\,\mathrm{d}x. \end{aligned} \tag{9}$$

After integrating by parts in the second and the third terms on the right-hand side of Eq. (9) and recalling that $\bar{w}$ satisfies the kinematic boundary conditions in Eq. (3), the governing equation for $\zeta(t)$ becomes

$$m\ddot{\zeta} + (k_0 + k_1)\zeta + k_2\zeta^3 = V^2 f_e(\zeta), \tag{10}$$

where

$$m = \varrho bh \int_0^\ell (\bar{w}(x))^2 \, \mathrm{d}x, \tag{11a}$$

$$k_0 = EI \int_0^\ell (\bar{w}''(x))^2 \, \mathrm{d}x, \tag{11b}$$

$$k_1 = N_0 \int_0^\ell (\bar{w}'(x))^2 \, \mathrm{d}x, \tag{11c}$$

$$k_2 = \frac{Ebh}{2\ell} \left(\int_0^\ell (\bar{w}'(x))^2 \, \mathrm{d}x \right)^2, \tag{11d}$$

$$f_e(\zeta) = \frac{1}{V^2} \int_0^\ell F_e(\zeta \bar{w}(x)) \bar{w}(x) \, \mathrm{d}x. \tag{11e}$$

Note that F_e is proportional to V^2, therefore f_e is independent of V. The left-hand side of Eq. (10) is comprised of the inertia force, $m\ddot{\zeta}$, and the restoring elastic force, $(k_0 + k_1)\zeta + k_2\zeta^3$, of the system, while the right-hand side represents the electrostatic force. Furthermore, $(k_0 + k_1)$ represents the stiffness of a linear elastic beam, and k_2 the strain-stiffening effect. The lumped electrostatic force depends on the adopted fringing field correction, and it cannot, in general, be expressed analytically.

The pull-in parameters are determined by discarding the inertia term in Eq. (10), and by requiring that the pull-in deflection and the pull-in voltage satisfy simultaneously the resulting nonlinear equation and the equation obtained by differentiating both sides of the resulting nonlinear equation with respect to ζ, i.e.,

$$(k_0 + k_1)\zeta + k_2\zeta^3 = V^2 f_e(\zeta), \tag{12a}$$

$$k_0 + k_1 + 3k_2\zeta^2 = V^2 \frac{\mathrm{d}f_e(\zeta)}{\mathrm{d}\zeta}. \tag{12b}$$

The pull-in deflection parameter ζ_{PI} is obtained by eliminating V^2 from Eqs. (12), and by numerically solving the resulting nonlinear algebraic equation in ζ. By substituting the so deduced value ζ_{PI} into Eq. (12a), the pull-in voltage V_{PI} is determined.

The fundamental frequency of the deflected beam at a given voltage $0 \leqslant \bar{V} < V_{\mathrm{PI}}$ is found as follows. We set $V = \bar{V}$ and $\ddot{\bar{\zeta}} = 0$ in Eq. (10), solve the resulting equation for $\bar{\zeta}$, set $\zeta = \bar{\zeta} + \Delta\zeta$ in Eq. (10), retain terms linear in $\Delta\zeta$, and assume that $\Delta\zeta = \Delta\zeta_0 \exp(\imath\omega t)$, where $\imath = \sqrt{-1}$ and ω is the frequency. Therefore, for every D.C. voltage $\bar{V}$ the fundamental frequency, in rad/s, of the deflected beam is given by

$$\omega(\bar{V}) = \left(\frac{1}{m} \left(k_0 + k_1 + 3k_2\zeta(\bar{V})^2 - \bar{V}^2 \frac{\mathrm{d}f_e}{\mathrm{d}\zeta}(\zeta(\bar{V})) \right) \right)^{1/2}. \tag{13}$$

The frequency $\omega(0)$ is the fundamental frequency of the prestressed undeflected beam. When the voltage $\bar{V}$ approaches the pull-in voltage V_{PI}, the frequency $\omega(\bar{V})$ drops rapidly to zero; see Ref. [1]. For $\bar{V} = V_{\mathrm{PI}}$ it follows from Eqs. (12b) and (13) that $\omega(V_{\mathrm{PI}}) = 0$. This is analogous to the following situation: at the onset of buckling of a prestressed beam, its fundamental frequency becomes zero.

As discussed in Ref. [1], the electrostatic force provides a softening effect on the overall mechanical stiffness, while the membrane stretching introduces strain hardening. The resonance frequency $\omega(\bar{V})$ is determined by a combination of these two opposite effects.

We choose

$$\bar{w}(x) = 16 \frac{g_0}{\ell^4} x^2 (x - \ell)^2. \tag{14}$$

Thus the trial function $\bar{w}(x)$ equals the static deflection of a fixed–fixed linear elastic microbeam resulting from the uniformly distributed load $384EIg_0/\ell^4$, chosen in such a way that $\bar{w}(\ell/2)=g_0$. Consequently Eqs. (11) become

$$m=\frac{128}{315}\varrho bhg_0^2\ell, \tag{15a}$$

$$k_0=\frac{1024}{5}\frac{EIg_0^2}{\ell^3}, \tag{15b}$$

$$k_1=\frac{512}{105}\frac{N_0g_0^2}{\ell}, \tag{15c}$$

$$k_2=\left(\frac{512}{105}\right)^2\frac{Ebhg_0^4}{2\ell^3}. \tag{15d}$$

The trial function given by Eq. (14) represents the actual deflection of the microbeam for small voltages. The present choice of $\bar{w}$ has been validated in Ref. [18], where the accuracy of the one degree-of-freedom model has been established by showing that its pull-in parameters agree well with those obtained by solving the integro-differential Eq. (1) with both the finite element, and the meshless local Petrov–Galerkin methods.

3.1. Comparison with the classical mass-spring system

The classical lumped one degree-of-freedom system equivalent to a microelectromechanical system is comprised of a parallel-plate capacitor, where both plates are rigid. The upper plate has mass m and is suspended by a linear spring of stiffness κ, and the bottom plate is held fixed. The electrostatic force given by the parallel-plate approximation acts on the movable electrode.

Neglecting effects of fringing fields, the initial stress, and the stiffening induced by geometric nonlinearities is equivalent to setting in Eq. (10) k_1 and k_2 equal to zero and $\mathscr{F}=1$. We thus get

$$m\ddot{\zeta}+k_0\zeta=V^2f_e(\zeta), \tag{16}$$

where

$$f_e(\zeta)=\frac{\varepsilon_0\varepsilon_r b}{2}\int_0^\ell\frac{\bar{w}(x)}{(g_0-\zeta\bar{w}(x))^2}\,\mathrm{d}x. \tag{17}$$

It follows from Eq. (13) that $\omega(\bar{V})$ equals zero when

$$k_0=\varepsilon_0\varepsilon_r b\bar{V}^2\int_0^\ell\frac{\bar{w}(x)^2}{(g_0-\zeta\bar{w}(x))^3}\,\mathrm{d}x, \tag{18}$$

which is equivalent to Eq. (12b) with k_1 and k_2 equal to zero and $\mathscr{F}=1$.

Recalling that k_0 given by Eq. (11b) depends upon $\bar{w}''$, $\bar{w}$ cannot be taken as a constant. Thus the present one degree-of-freedom model differs from the classical lumped mass-spring system that gives $\|w_{\mathrm{PI}}\|_\infty=g_0/3$ and $V_{\mathrm{PI}}^2=8\kappa/(27\varepsilon_0\varepsilon_r A)$, where A is the plate area.

4. Three dimensional finite-element analysis

Results from the one degree-of-freedom model presented in Section 3 are compared with those from the 3-D finite element simulations performed with the commercial code ANSYS. Predictions from 3-D simulations are considered more reliable since they do not involve a priori assumptions on the electrostatic force and the kinematics of beam's deformations. Details of simulating MEMS problems with ANSYS are given in Ref. [22]. Following these guidelines we used the ROM144, a directly coupled electrostatic and structural field tool utilizing a 2-D or 3-D reduced order model based on a modal representation of the structural response. The ROM144 element has several modal degrees of freedom including modal displacements, electrical potential, and nodal displacements. In Ref. [23], the finite element findings of ROM144 tool have been found to agree well with experimental results. We modified the "Sample Miniature

Table 1
Geometric and material parameters for the problems studied

Parameters	Values
ℓ, [μm]	25
b, [μm]	0.25
h, [μm]	0.5
g_0, [μm]	1
ϱ, [kg/m^3]	2329
E, [GPa]	169
ν	0.066
ε_r	1

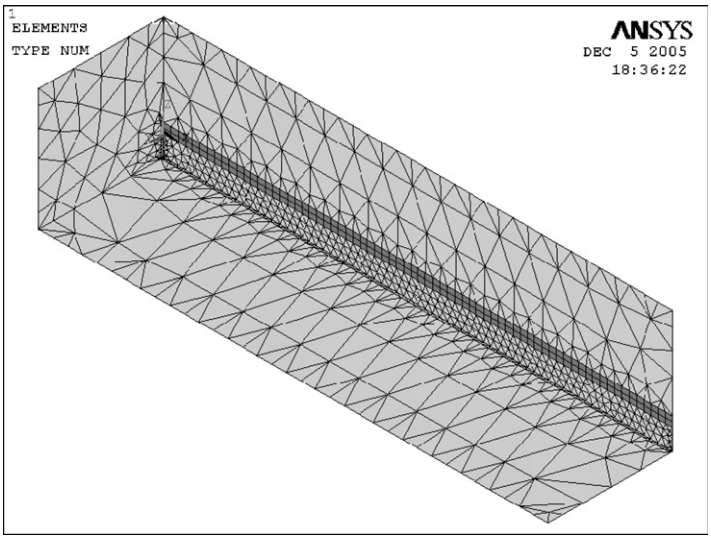

Fig. 2. Schematics of the 3-D finite element mesh used for simulations of the clamped–clamped beam with the commercial code ANSYS. The domain in light grey is the dielectric, and the one in dark grey is the microbeam.

Clamped–Clamped Beam Analysis'', example 6.6 of the Section ''Coupled-Field Analysis Guide'' in Ref. [24], adapting it to a narrow microbeam by extending the surrounding dielectric in order to accurately simulate fringing fields. The material and geometric parameters of the narrow microbeam analyzed with ANSYS are listed in Table 1. The finite element mesh is shown in Fig. 2. For the microbeam studied, $\ell/h = 50$, $h/g_0 = 0.5$, and $h/b = 2$.

Deformations of only one-half of the system are analyzed due to symmetry conditions, and a fine mesh is employed in the gap region. In particular, the dielectric medium is considered as a block of length 25 μm, half-width 6 μm, and thickness 6 μm. The elements SOLID 45 (8-node brick elements) are used to discretize the microbeam, while SOLID 122 (20-node tetrahedral elements) are used to divide the dielectric region. Geometric nonlinearities are included in the analysis. Here we retain the optimized mesh and the dielectric region found in Ref. [18] for extracting the pull-in parameters, with the microbeam domain subdivided into 70, 2 and 2 elements in the axial, the width, and the thickness directions respectively.

The fundamental natural frequency of the system is obtained by first performing a static analysis to determine the deformed shape of the clamped–clamped narrow microbeam under a given applied voltage. Subsequently, harmonic analysis is performed by exciting the deflected/prestressed beam via a small (the amplitude of the A.C. voltage equals ~5% of the D.C. voltage) harmonic voltage, and computing the amplitude of oscillations at the beam mid-span for excitation frequencies increased in increments of 5 kHz.

5. Results and comparisons

5.1. One degree-of-freedom model

The proposed electromechanical model for a narrow clamped–clamped microbeam has been validated by computing results for a microbeam with material and geometric parameters listed in Table 1, and comparing computed results with those obtained from 3-D finite element simulations performed with ANSYS; see Section 4. For this geometry, both the effect of fringing fields due to the thickness of the microbeam ($h/b = 2$), and the effect of the membrane stretching correction due to large displacement of the microbeam ($g_0/h = 2$) are relevant. Three different values of the initial stress σ_0, representative of pretensioned, stress-free and precompressed beams, have been examined. The initial stress may be induced during the fabrication process. We also present in Tables 3–6 results from models proposed in Refs. [1,7,16], and have summarized key features of these works in Table 2. Results presented herein are our calculations with assumptions made in Refs. [1,7,16].

As representative comparison parameters we choose the pull-in D.C. voltage $V_{\rm PI}$, the pull-in maximum deflection $\|w_{\rm PI}\|_\infty \equiv \zeta_{\rm PI}\bar{w}(\ell/2)$, the maximum frequency $\omega_{\max}$ attained for $\bar{V}$ spanning the interval $(0, V_{\rm PI})$, and the voltage $V_{\omega_{\max}}$ corresponding to $\omega_{\max}$.

It is clear from the results given in Table 3 that the fundamental frequency of the microbeam computed from Eq. (13) with $\bar{V} = 0$ agrees very well with that computed with ANSYS. Figs. 3–5 report the variation of the fundamental frequency $\omega(\bar{V})$ normalized with respect to the fundamental frequency $\omega(0)$ of the undeflected microbeam, versus the applied voltage V in the range $(0, V_{\rm PI})$, normalized with respect to the pull-in voltage $V_{\rm PI}$. Variables for each curve are normalized with respect to the corresponding parameters listed in Tables 4–6. Values in Tables give quantitative differences among model predictions and finite element results. Figs. 3–5 show qualitative differences among the results. In Fig. 4, $\omega_{\max}/\omega(0)$ and $V_{\omega_{\max}}/V_{\rm PI}$ for the assumptions of Ref. [7] are depicted, where $V_{\rm PI}$ is the corresponding pull-in voltage reported in Table 5.

Results presented in Tables 4–6 and Figs. 3–5 show that for a narrow microbeam undergoing relatively large displacements, there are significant discrepancies between the pull-in parameters, and the maximum frequencies computed with the models proposed in Refs. [1,7,16] and the 3-D finite element solution. When completely discarding fringing field effects as proposed in Ref. [1], the electrostatic force is underestimated resulting in an overestimation of the pull-in voltage and an underestimation of the pull-in displacement. As a consequence the displacements predicted for a microbeam are smaller than the actual ones and the strain

Table 2
Key features of different electromechanical models

Model	Membrane stretching	Capacitance approximation
Ref. [1]	Yes	Parallel plate
Ref. [16]	No	Palmer's
Ref. [7]	Yes	Palmer's
Present work	Yes	Eq. (5)

Table 3
Comparison of the fundamental frequency of the microbeam with no voltage applied computed from Eq. (13) with that computed with ANSYS

σ_0, [MPa]	$\omega(0)/2\pi$	[MHz]
	ANSYS	Eq. (13)
100	8.300	8.301
0	7.000	7.029
−100	5.300	5.468

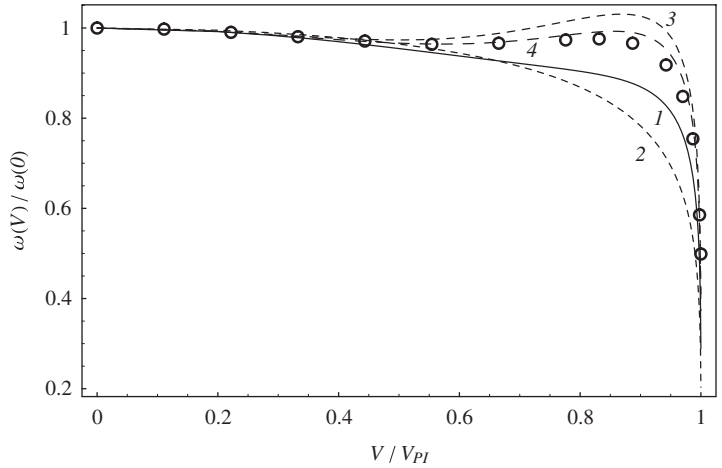

Fig. 3. Variation of the fundamental frequency with applied D.C. voltage for $\sigma_0 = 100$ MPa computed with ANSYS (open circles), and the electromechanical models of Ref. [1] (curve 1), Ref. [16] (curve 2), Ref. [7] (curve 3), and the present work (curve 4).

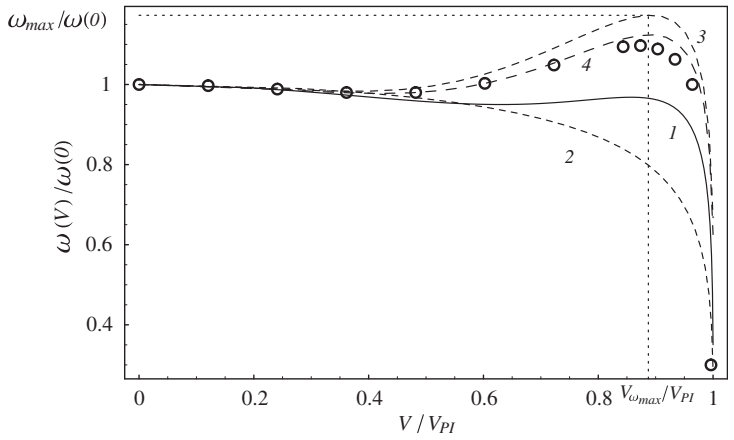

Fig. 4. Variation of the fundamental frequency with applied D.C. voltage for $\sigma_0 = 0$ MPa computed with ANSYS (open circles), and the electromechanical models of Ref. [1] (curve 1), Ref. [16] (curve 2), Ref. [7] (curve 3), and the present work (curve 4).

hardening due to membrane stretching is underestimated. Therefore, the membrane stretching is incapable of dominating the electrostatic softening for pretensioned microbeams as illustrated by results plotted in Fig. 3 where the frequency vs. voltage curve is monotonically decreasing. When fringing field effects due to the microbeam finite width are also considered as has been done in Ref. [7], the pull-in voltage and the pull-in maximum deflection are slightly overestimated, resulting in an overestimation of the strain hardening versus the electrostatic softening. The maximum value of the fundamental frequency is therefore overestimated and the frequency versus voltage curve shows a relevant overshoot with respect to the finite element solution. The work included in Ref. [16] neglects the strain hardening effect and always gives monotonic behavior of the frequency versus the voltage response. In addition, the neglect of the strain hardening effect underestimates the microbeam stiffness and the pull-in parameters. The present electromechanical model based on the fringing fields correction in Eq. (7) provides accurate quantitative predictions of the pull-in parameters and the maximum frequency for narrow microbeams and reliably captures the qualitative behavior of the lowest frequency versus the applied D.C. voltage.

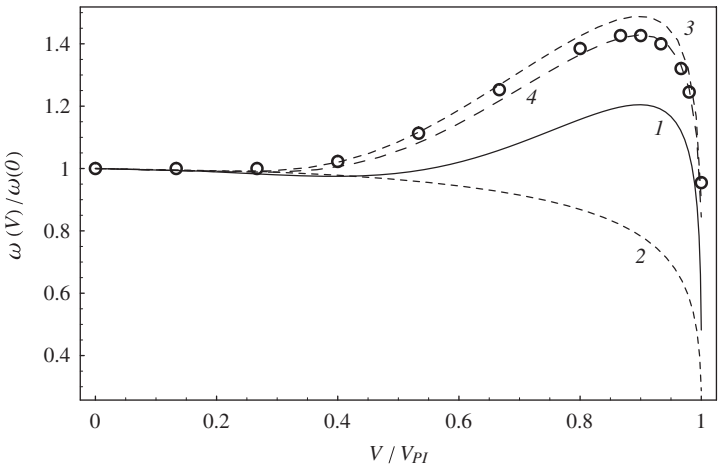

Fig. 5. Variation of the fundamental frequency with applied D.C. voltage for $\sigma_0 = -100$ MPa computed with ANSYS (open circles), and the electromechanical models of Ref. [1] (curve 1), Ref. [16] (curve 2), Ref. [7] (curve 3), and the present work (curve 4).

Table 4
For $\sigma_0 = 100$ MPa, comparison of representative parameters found using different electromechanical models and 3-D finite element simulations

	ANSYS	One degree-of-freedom model			
		Ref. [1]	Ref. [16]	Ref. [7]	Present work
$\|w_{PI}\|_\infty$, [μm]	0.618	0.532	0.491	0.637	0.621
V_{PI}, [V]	226	378	196	251	236
$\omega_{max}/2\pi$, [MHz]	8.300	8.301	8.301	8.556	8.301
$V_{\omega_{max}}$, [V]	0	0	0	219	0

Table 5
For $\sigma_0 = 0$ MPa, comparison of representative parameters found using different electromechanical models and 3-D finite element simulations

	ANSYS	One degree-of-freedom model			
		Ref. [1]	Ref. [16]	Ref. [7]	Present work
$\|w_{PI\|_\infty}$, [μm]	0.642	0.560	0.491	0.658	0.644
V_{PI}, [V]	208	343	166	231	217
$\omega_{max}/2\pi$, [MHz]	7.680	7.029	7.029	8.243	7.899
$V_{\omega_{max}}$, [V]	181	0	0	204	194

Table 6
For $\sigma_0 = -100$ MPa, comparison of representative parameters found using different electromechanical models and 3-D finite element simulations

	ANSYS	One degree-of-freedom model			
		Ref. [1]	Ref. [16]	Ref. [7]	Present work
$\|w_{PI}\|_\infty$, [μm]	0.660	0.597	0.491	0.683	0.671
V_{PI}, [V]	188	306	129	210	197
$\omega_{max}/2\pi$, [MHz]	7.560	6.587	5.468	8.138	7.810
$V_{\omega_{max}}$, [V]	163	275	0	186	176

From the analysis of the data reported in Figs. 3–5, we conclude that the pretension in the microbeam reduces effects of the D.C. voltage on the lowest frequency before the pull-in instability occurs, while the precompression enhances the nonmonotonic behavior of the lowest frequency versus the D.C. voltage.

We note that the pull-in voltage of ~230 V found for the microbeam studied herein is less than the breakdown voltage of ~520 V for a silicon-to-silicon configuration analyzed by Ono et al. [25].

5.2. Validation of the one degree-of-freedom model

An approximate solution of the problem defined by Eqs. (1), (2), (6) and boundary conditions in Eq. (3) by the multimode analysis [1,9] is found by expressing the displacement field $w(x,t)$ as

$$w(x,t) = \boldsymbol{\psi}(x)\boldsymbol{\zeta}(t), \tag{19}$$

where $\boldsymbol{\psi}$ is a row N-vector containing the eigenfunctions of the fixed–fixed beam (see Ref. [26]), and $\boldsymbol{\zeta}$ is the column N-vector of unknowns (modal amplitudes). Substituting from Eq. (19) into Eq. (1), premultiplying both sides by $\boldsymbol{\psi}^{\mathrm{T}}$ and integrating over the beam span yields

$$\begin{aligned}&\int_0^\ell \varrho bh\boldsymbol{\psi}^{\mathrm{T}}\boldsymbol{\psi}\ddot{\boldsymbol{\zeta}}\,\mathrm{d}x + \int_0^\ell EI\boldsymbol{\psi}^{\mathrm{T}}\boldsymbol{\psi}^{IV}\boldsymbol{\zeta}\,\mathrm{d}x\\ &\quad - \left(\frac{Ebh}{2\ell}\int_0^\ell \boldsymbol{\zeta}^{\mathrm{T}}(\boldsymbol{\psi}')^{\mathrm{T}}\boldsymbol{\psi}'\boldsymbol{\zeta}\mathrm{d}x + N_0\right)\int_0^\ell \boldsymbol{\psi}^{\mathrm{T}}\boldsymbol{\psi}''\boldsymbol{\zeta}\,\mathrm{d}x\\ &\quad = \int_0^\ell F_e(\boldsymbol{\psi}\boldsymbol{\zeta})\boldsymbol{\psi}^{\mathrm{T}}\,\mathrm{d}x.\end{aligned} \tag{20}$$

After integrating by parts and exploiting the fact that the eigenfunctions satisfy the kinematic boundary conditions in Eq. (3) we obtain the following set of nonlinear coupled ordinary differential equations:

$$\mathbf{m}\ddot{\boldsymbol{\zeta}} + \mathbf{k}(\boldsymbol{\zeta})\boldsymbol{\zeta} = V^2\mathbf{f}_e(\boldsymbol{\zeta}), \tag{21}$$

where

$$\mathbf{m} = \int_0^\ell \varrho bh\boldsymbol{\psi}^{\mathrm{T}}\boldsymbol{\psi}\,\mathrm{d}x, \tag{22a}$$

$$\mathbf{k}(\boldsymbol{\zeta}) = \int_0^\ell (EI(\boldsymbol{\psi}'')^{\mathrm{T}}\boldsymbol{\psi}'' + N_0(\boldsymbol{\psi}')^{\mathrm{T}}\boldsymbol{\psi}')\,\mathrm{d}x + \left(\frac{Ebh}{2\ell}\int_0^\ell \boldsymbol{\zeta}^{\mathrm{T}}(\boldsymbol{\psi}')^{\mathrm{T}}\boldsymbol{\psi}'\boldsymbol{\zeta}\,\mathrm{d}x\right)\int_0^\ell (\boldsymbol{\psi}')^{\mathrm{T}}\boldsymbol{\psi}'\,\mathrm{d}x, \tag{22b}$$

$$\mathbf{f}_e(\boldsymbol{\zeta}) = \frac{1}{V^2}\int_0^\ell F_e(\boldsymbol{\psi}\boldsymbol{\zeta})\boldsymbol{\psi}^{\mathrm{T}}\,\mathrm{d}x. \tag{22c}$$

Eqs. (21) are coupled because the stiffness matrix $\mathbf{k}(\boldsymbol{\zeta})$ is nondiagonal, and its components and the components of the electrostatic load vector $\mathbf{f}_e(\boldsymbol{\zeta})$ are nonlinear functions of $\boldsymbol{\zeta}$.

The pull-in parameters are extracted by discarding the inertia term in Eq. (21) and by solving the resulting system of equations with the displacement iteration pull-in extraction (DIPIE) algorithm [20]. The displacement $w(\ell/2)$ at the beam's mid-span is chosen as the driving parameter (see Ref. [20]). The pull-in

Table 7
Pull-in parameters from multi-mode analysis of the present set of electromechanical equations with increasing number of modes, N

N	$\sigma_0 = 100$ MPa		$\sigma_0 = 0$ MPa		$\sigma_0 = -100$ MPa	
	$\|w_{\mathrm{PI}}\|_\infty$, [μm]	V_{PI}, [V]	$\|w_{\mathrm{PI}}\|_\infty$, [μm]	V_{PI}, [V]	$\|w_{\mathrm{PI}}\|_\infty$, [μm]	V_{PI}, [V]
1	0.62	238	0.65	218	0.67	198
3	0.62	237	0.64	217	0.67	197
5	0.62	236	0.64	217	0.67	196

parameters computed with increasing number of modes for three values of the prestress are listed in Table 7. It is clear that the consideration of only one mode in Eq. (19) gives sufficiently accurate values of the pull-in voltage and the pull-in deflection. The little difference between values obtained with one, three and five modes evinces that the participation of modes other than the first can be neglected. This validates the single degrees-of-freedom model presented in Section 3. A comparison of values listed in Tables 4–6 with those given in Table 7 shows good agreement between the pull-in parameters from the one degree-of-freedom model of Section 3, and those computed with the multimode analysis combined with the DIPIE algorithm. Thus the use of either the first mode function or Eq. (14) giving the static deflection of a beam loaded with a uniformly distributed force gives equally good results.

5.3. Remarks

The reduced order models for clamped rectangular, circular and elliptic plates and membranes incorporating the effect of the Casimir force are given in Refs. [29–31].

6. Conclusions

We have studied vibrations of a narrow microbeam predeformed by the electric field due to a D.C. voltage difference between the microbeam and the parallel rigid flat conductor. It is shown that the proposed electromechanical model, based on improved estimates of the electrostatic fringing fields accurately predicts the vibrational response of the microbeam. For relatively large gaps between the microbeam and the base rigid conductor both the membrane stretching and the fringing field effects are important, and neglecting one of them may result in improper estimates of both the pull-in parameters and the resonance frequencies. The combination of strain hardening introduced by the membrane stretching and of the electrostatic softening strongly affect the microbeam resonance frequencies. A proper estimate of fringing fields is essential for accurately predicting frequencies of the deflected narrow microbeam.

References

[1] E.M. Abdel-Rahman, M.I. Younis, A.H. Nayfeh, Characterization of the mechanical behavior of an electrically actuated microbeam, *Journal of Micromechanics and Microengineering* 12 (6) (2002) 759–766.
[2] A.H. Nayfeh, M.I. Younis, Dynamics of MEMS resonators under superharmonic and subharmonic excitations, *Journal of Micromechanics and Microengineering* 15 (2005) 1840–1847.
[3] J.F. Rhoads, S.W. Shaw, K.L. Turner, The nonlinear response of resonant microbeam systems with purely-parametric electrostatic actuation, *Journal of Micromechanics and Microengineering* 16 (2006) 890–899.
[4] H.A. Tilmans, R. Legtenberg, Electrostatically driven vacuum-encapsulated polysilicon resonators, part II: theory and performance, *Sensors and Actuators A* 45 (1) (1994) 67–84.
[5] M.I. Younis, A.H. Nayfeh, A study of the nonlinear response of a resonant microbeam to an electric actuation, *Nonlinear Dynamics* 31 (2003) 91–117.
[6] S. Krylov, R. Maimon, Pull-in dynamics of an elastic beam actuated by continuously distributed electrostatic force, *Journal of Vibration and Acoustics* 126 (2004) 332–342.
[7] J.-H. Kuang, C.-J. Chen, Dynamic characteristics of shaped micro-actuators solved using the differential quadrature method, *Journal of Micromechanics and Microengineering* 14 (4) (2004) 647–655.
[8] W.C. Xie, H.P. Lee, S.P. Lim, Nonlinear dynamic analysis of MEMS switches by nonlinear modal analysis, *Nonlinear Dynamics* 31 (2003) 243–256.
[9] Y. Zhang, Y.-p. Zhao, Numerical and analytical study on the pull-in instability of micro-structure under electrostatic loading, *Sensors and Actuators A* 127 (2006) 366–380.
[10] J.D. Zook, D.W. Burns, H. Guckel, J.J. Sniegowski, R.L. Engelstad, Z. Feng, Characteristics of polysilicon resonant microbeams, *Sensors and Actuators A* 35 (1992) 290–294.
[11] G.I. Taylor, The coalescence of closely spaced drops when they are at different electric potentials, *Proceedings of the Royal Society A* 306 (1968) 423–434.
[12] H.C. Nathanson, W.E. Newell, R.A. Wickstrom, J.R. Davis, The resonant gate transistor, *IEEE Transactions on Electron Devices* 14 (3) (1967) 117–133.
[13] J.A. Pelesko, D.H. Bernstein, *Modeling MEMS and NEMS*, Chapman & Hall, 2002, (Chapter 7).
[14] A. Fargas Marquès, R.Costa Castelló, A.M. Shkel, Modelling the electrostatic actuation of MEMS: state of the art 2005, Technical Report (2005). ⟨http://bibliotecnica.upc.es/reports/ioc/IOC-DT-P-2005-18.pdf⟩.

[15] H.B. Palmer, Capacitance of a parallel-plate capacitor by the Schwartz–Christoffel transformation, *Transactions of the American Institute of Electrical Engineers* 56 (3) (1937) 363–366.
[16] P.M. Osterberg, S.D. Senturia, M-TEST: a test chip for MEMS material property measurement using electrostatically actuated test structures, *Journal of Microelectromechanical Systems* 6 (2) (1997) 107–118.
[17] S. Pamidighantam, R. Puers, K. Baert, H.A.C. Tilmans, Pull-in voltage analysis of electrostatically actuated beam structures with fixed-fixed and fixed-free end conditions, *Journal of Micromechanics and Microengineering* 12 (4) (2002) 458–464.
[18] R.C. Batra, M. Porfiri, D. Spinello, Electromechanical model of electrically actuated narrow microbeams, *Journal of Microelectromechanical Systems* 15 (5) (2006) 1175–1189.
[19] M.I. Younis, E.M. Abdel-Rahman, A.H. Nayfeh, A reduced-order model for electrically actuated microbeam-based MEMS, *Journal of Microelectromechanical Systems* 12 (5) (2003) 672–680.
[20] O. Bochobza-Degani, D. Elata, Y. Nemirovsky, An efficient DIPIE algorithm for CAD of electrostatically actuated MEMS devices, *Journal of Microelectromechanical Systems* 11 (5) (2002) 612–620.
[21] L.D. Landau, E.M. Lifshitz, *Theory of Elasticity*, Pergamon Press, New York, 1986.
[22] R.J. Shapoorabadi, A.G. Kirk, Comparison of three finite element models for analysis of MEMS micromirrors, in: J.C. Armitage, S.Fafard, R.A. Lessard, G.A. Lampropoulos (Eds.), *Proceedings of SPIE, International Conference on Applications of Photonic Technology*, in Photonics North: Optical Components and Devices, Vol. 5577, Ottawa, Canada, September 2004, pp. 849–859.
[23] H. Toshiyoshi, H. Fujita, Electrostatic micro torsion mirrors for an optical switch matrix, *Journal of Microelectromechanical Systems* 5 (1996) 231–237.
[24] ANSYS, *ANSYS Release 8.0 Documentation*, ANSYS Inc. (2003).
[25] T. Ono, D.Y. Sim, M. Esashi, Micro-discharge and electric breakdown in a micro-gap, *Journal of Micromechanics and Microengineering* 10 (2000) 445–451.
[26] L. Meirovitch, *Fundamentals of Vibrations*, McGraw-Hill, New York, 2001.
[27] R.C. Batra, M. Porfiri, D. Spinello, Review of modeling electrostatically actuated microelectromechanical systems, *Smart Materials and Structures*, accepted for publication.
[28] R.C. Batra, M. Porfiri, D. Spinello, Capacitance estimate for electrostatically actuated narrow microbeams, *Micro and Nano Letters* 1 (2006) 71–73.
[29] R.C. Batra, M. Porfiri, D. Spinello, Reduced-order models for microelectromechanical rectangular and circular plates incorporating the Casimir force, submitted for publication.
[30] R.C. Batra, M. Porfiri, D. Spinello, Vibrations and pull-in instabilities of microelectromechanical von Kármán elliptic plates incorporating the Casimir force, submitted for publication.
[31] R.C. Batra, M. Porfiri, D. Spinello, Effects of Casimir force on pull-in instability in micromembranes, *Europhysics Letters* 77 (2007) Art. No. 20010.